Rapid Acquisition and Return of Mercury Polar Ice Samples

Emmett V. Leader[1], Liba A. Snyder[2]
Christy D. Renteria Vidal[3]
and
Javid Bayandor[4]

***CR**ashworthiness for **A**erospace **S**tructures and **H**ybrids Laboratory* (*The **CRASH** Lab*)|©
University at Buffalo – The State University of New York, Buffalo, NY, 14260

To this date only two missions have visited Mercury, with a third currently on its way. None of these have touched down on the surface, leaving Mercury the least studied of the inner planets. Preliminary results suggest that there may be water ice in the permanently shaded regions of craters near Mercury's north pole, which holds many interesting implications for the formation of the planet and history of the early Solar System. It is the goal of the High-speed Extraction and Retrieval for Mercury's Extraterrestrial Samples mission, or HERMES, to make the journey to Mercury and retrieve accreted polar ice samples so that scientists on Earth may unlock its secrets. To accomplish this, HERMES will have to act quickly in order to carry out its task, as the extreme conditions on and around the surface of Mercury make long-term operations difficult. After entering a polar orbit, a lander will descend to the surface, collect samples, load them into a cryocooler, and launch an ascent vehicle to rendezvous with an orbiter, all within the span of about two hours. This would make HERMES both the first mission to the surface of Mercury, as well as the first mission to return samples to Earth from another planet, containing a wealth of information about the composition and formation of Mercury's polar ice.

Nomenclature

A	=	amplitude of oscillation
a	=	cylinder diameter
C_p	=	pressure coefficient
Cx	=	force coefficient in the x direction
Cy	=	force coefficient in the y direction
dt	=	time step
e_{offset}	=	eccentricity from ideal drill axis
F_{drill}	=	drilling reaction force vector
F_{ext}	=	external load vector at end effector
$F_{friction}$	=	frictional force
F_{insert}	=	required insertion force
$F_{misalign}$	=	force due to misalignment
$F_{preload}$	=	spring or latch preload force
F_{thrust}	=	axial drilling thrust force
f_{rpl}	=	feed rate per revolution length
Fx	=	X component of the resultant pressure force acting on the vehicle
Fy	=	Y component of the resultant pressure force acting on the vehicle
f, g	=	generic functions
$g_{Mercury}$	=	Mercury surface gravitational acceleration
h	=	height
i	=	time index during navigation
I_j	=	joint rotational inertia
I_{sp}	=	specific impulse
j	=	waypoint index
k	=	thermal conductivity
L	=	link length
m_{drill}	=	drill assembly mass
m_{link}	=	individual link mass

[1] Undergraduate Student, The CRASH Lab, Dept. of Mechanical and Aerospace Eng.
[2] Undergraduate Student, The CRASH Lab, Dept. of Mechanical and Aerospace Eng.
[3] Undergraduate Student, The CRASH Lab, Dept. of Mechanical and Aerospace Eng.
[4] Faculty Advisor, Funder & Director, The CRASH Lab, Dept. of Mechanical and Aerospace Eng., AIAA Associate Fellow.

m_0 = initial mass
m_f = final mass
m_p = propellant mass
N = normal reaction force
Q_{rad} = radiative heat load
r_j = moment arm vector from joint j to point of force application
$T_{drill,reaction}$ = drilling-induced reaction torque
$T_{friction}$ = frictional torque loss in joint
T_j = required actuator torque at joint j
T_{rack} = rack temperature
T_{rotary} = peak rotational drilling torque
T_{sur} = surrounding temperature
α_j = max angular acceleration at joint j
ε_{eff} = effective emissivity
Δh = incremental drilling depth
ΔV = velocity change
μ = coefficient of friction
σ = Stefan-Boltzmann constant
$\sum t$ = cumulative drilling time

I. Introduction

This paper details the mission architecture for the retrieval and return of ice samples from Mercury's polar regions. The main goal of the mission is to retrieve a selection of samples from various depths, with a total mass of 1 kg, from the permanently shaded region of a crater near the planet's north pole. These samples must then be safely sent to Mercury orbit and then on to Earth, all the way preserving the original conditions the samples were retrieved in as well as possible for study on Earth. In addition to the sample collection, other scientific data will be collected during the mission, taking advantage of the proximity to Mercury and the Sun to collect data both in orbit and on the surface. This mission aims to prove that it is possible to perform both a sample collection and return with just a single launch, potentially paving the way for other such missions on Mercury as well as other bodies in the solar system.

II. Impact

The origins of ice in Mercury's permanently shaded craters are a mystery. NASA's MESSENGER mission detected signs of ice in craters located near Mercury's poles, but the actual composition, surface characteristics, and process of formation remain unknown. Current data suggests that these permanently shaded craters have surfaces partially or fully composed of ice at a temperature of about –150 °C, though until a mission is sent to investigate further this is not known for sure. This is the purpose of the HERMES mission, to shed light on the mysteries hidden in these permanently shaded craters. By collecting ice samples from these regions and returning them to Earth, the mission would allow scientists to begin learning about these interesting formations and what they may reveal about the conditions of Mercury at present and the distant past, possibly as far back as the formation of the Solar System.

In addition to the collection of the ice samples, the HERMES craft will have a unique opportunity to perform other science while on the surface and in orbit. The lander will be equipped with various instruments, such as a seismometer to measure any activity beneath Mercury's surface, and a magnetometer to measure the influence of solar winds on the small planet. Additionally, the time spent in orbit around the closest planet to the Sun would be a prime opportunity to collect data on solar weather.

In addition to the scientific discoveries that this mission would pioneer, HERMES would also serve as a test bed for a new type of mission architecture capable of collecting and returning samples with a single mission. Should it prove successful, it can be adapted to missions to many other bodies in the Solar System, such as the moons of the gas giants or even asteroids. These sample return missions could inform us about the origins of the bodies in the Solar System, as well as collecting data to aid in planning for and operating future missions.

III. Mission Architecture

To obtain samples of water ice HERMES must complete its journey to and from Mercury. The mission begins with an initial launch from Earth's surface in 2032, when Earth in line with Venus. This initial launch requires Earth and Venus orbits to be synced which happens approximately once every eight years, and the indicated year is the earliest launch time available. Once launched, a single flyby of Earth is done to conserve fuel for the Venus flybys which will occur later in the journey to Mercury. HERMES will reach Venus sometime between 2033-2034 and drop its orbit to do two flybys around Venus. These flybys are necessary to allow HERMES to change the perihelion of its orbit to roughly the same distance as Mercury's orbit around the Sun [14]. Once the desired orbital size is reached, the thrust

toward Mercury is achieved, two more flybys are executed around Mercury to reduce the speed so that HERMES can arrive at the desired parking orbit around the planet. The approximate date for this parking orbit to begin would be around 2036-2037 and would be a polar orbit around Mercury. The parking orbit for where the descent and ascent module will release and connect, respectively, is going to have an altitude of 480km above the north pole of Mercury with approximately a 2.3-hour orbital period. The ideal timeline of sample collection would be within one orbit, but more orbits can be considered if deemed necessary. In order to drop into direct free fall above the desired landing zone, the velocity change of the descent module needs to be 2.996km/s. Once entering free fall the time spent thrusting will be dependent on the total mass of the module itself. Figure 1 shows the thrust per kg required to land in a desired crater of water ice based on the time spent free falling before the power descent phase.

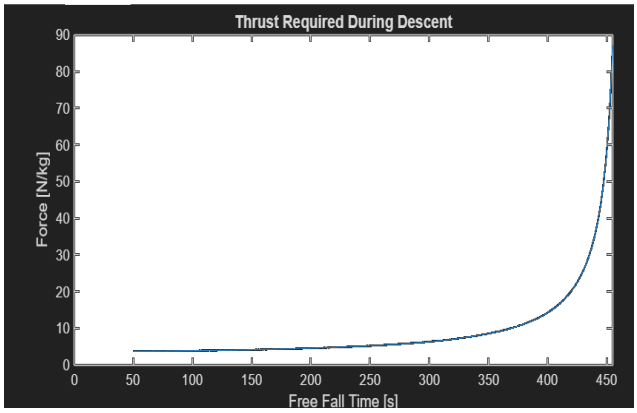

Figure 1: Required thrust for descent module dropping out of polar orbit

After landing the sample collection process will occur and from there the sample must then be returned to Earth for further analysis. To leave the surface of Mercury, the ascent module must complete an orbital insertion where it starts with a vertical launch and then maneuver to rendezvous with the orbiter with the aim of completing the return trajectory. To get from surface back to polar orbit a total velocity change of 4.717km/s will be necessary to ensure proper rendezvous. Once attached with the orbiter, the samples will be loaded into the return vehicle and the first step on the return trajectory is going to be an exit from Mercury polar orbit into a transfer orbit between Mercury and Venus. The change in velocity required for this orbital maneuver is approximately 3.281km/s. After thrusting into the transfer orbit two more Venus flybys will be executed to begin the transfer orbit towards Earth. During the final transfer orbit from Venus to Earth a final Earth flyby will be carried out in order to slow the orbiter down to drop into a parking orbit around Earth. Once in the orbit around Earth, analysis will be conducted to assess the optimal time and place for the capsule containing the samples to be dropped out of the Earth parking orbit for retrieval.

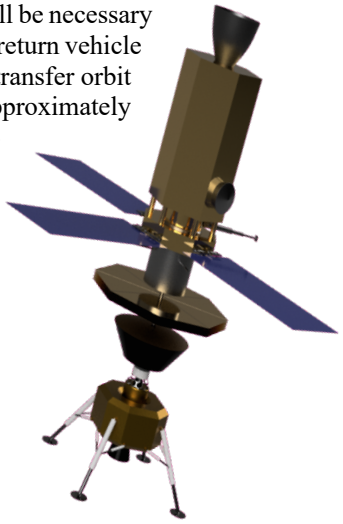

Figure 2: HERMES mission concept showing integrated lander and orbiter configuration during Mercury transit phase

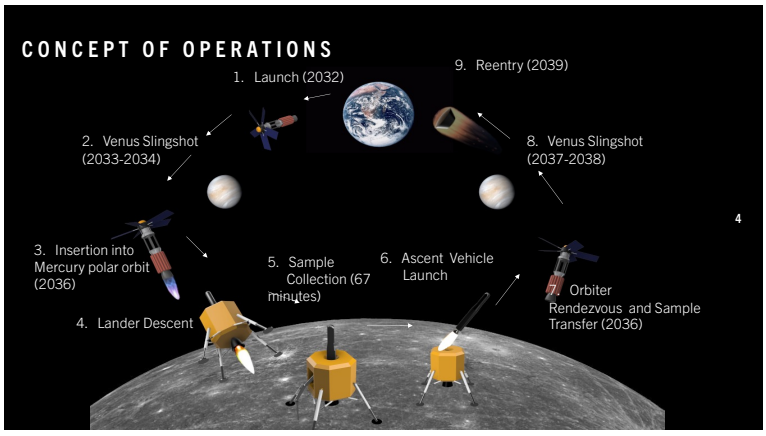

Figure 3: Mission sequence from Earth launch to sample return.

IV. Orbiter

A. System Architecture

The orbiter serves the vital purpose of transporting the mission components to Mercury, inserting them into a polar orbit, sending the lander down to the surface, and finally performing a rendezvous with the ascent vehicle to collect the samples and prepare them for the journey to Earth. All of these tasks must be performed in addition to gathering scientific data and serving as a communications relay between Earth and the mission subsystems on the surface. The orbiter will use X-band antennas that were similarly used by BepiColombo as these are able to withstand the intense environment surrounding Mercury.[13] These antennas will communicate with earth via the Deep Space Network (DSN).[12] The control hub will also handle trajectory as well as navigation to and from Mercury as well as from orbit to Mercury. While the sample is being collected, the various instruments will study Mercury and collect more information. GNC will control the transport of the lander as well as its rendezvous. After samples are collected and secured the GNC will return to Earth.

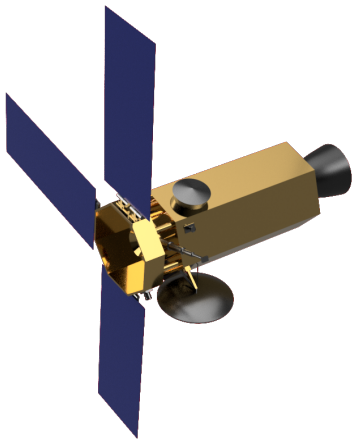

Figure 4: HERMES orbiter spacecraft

B. Structures and Mechanisms

The lander will be transported in a "stacked together" system with the orbiter at the bottom and the lander on top. This physical arrangement is used by Chandrayaan-2 to withstand launch vibrations and maintain its structural integrity as well as maximize fuel.[2] Once the lander reaches Mercury, the lander is released using a spin eject device, this is inspired by the Cassini-Huygens mission which used pyrobolts and helical rails to release the lander and make it rotate to stabilize the lander. This design uses a similar design but differs in using pyrobolts. The orbiter will use motorized latches to hold the lander and use springs to push it. These springs must align perfectly to allow the lander to be pushed with accuracy. This also uses helical rails to have the lander spin and keep it stable to land exactly. [3][4][7]

Once the samples are collected, the ascent vehicle will rendezvous with ascent vehicle using lidar technology. This technology is widely used by various missions including NASA's Orion and SpaceX Dragon/ISS docking. Lidar is able to range where the orbiter is using light (laser). The lander illuminates the area to determine the location of the orbiter and measures how long the light takes to return to the sensor. The sensor that will be used for this mission is a flash lidar, it requires no moving parts, which is perfect for long journeys. This type of lidar flashes a light once to capture the entire scene to know the exact location and distance of the orbiter.[8] Once the ascent vehicle reaches the orbiter, it will be connected via the motorized latches and will then secure the samples and safely seal them, the orbit will begin its journey to earth.[6][5] Once it reaches earth, the samples will be sent to earth and return using a parachute.

C. Power System

The power system consists of solar arrays made to withstand the high thermal environment of Mercury. Following the design Optical Solar Reflector (OSR) MESSENGER uses, the solar arrays are composed of 30% solar cells and 70% mirrors to prevent the internal components from overheating. The solar cells are composed of Triple-Junction Gallium Arsenide (GaAs) as these can handle high temperatures. The mirrors will be coated with a high-emissivity silica to reflect the sun's heat and radiate its internal heat. The solar arrays will also be tilted using a two-axis rotation to maintain internal temperature from rising and keep internal components at a stable temperature to function properly.[9][10]

V. Lander Design Details

A. System Architecture

The HERMES lander is designed as a compact surface platform whose primary functions are (i) safe delivery of the surface sampling payload to Mercury's north polar region, (ii) execution of a rapid sample acquisition sequence within the permanently shaded environment, and (iii) provision of mechanical, thermal, and operational support for ascent vehicle launch and sample transfer back to the orbiter. The HERMES Mission architecture comprises an orbiter, lander, ascent vehicle, and return vehicle. The lander specifically houses the robotic arm and ascent vehicle launch system, while providing the cryogenic preservation pathway that maintains sample collection conditions through transfer operations.

Because the HERMES Mission targets ice-bearing material in permanently shaded regions, the lander architecture is driven by two competing requirements: (1) minimize mission duration on the surface to reduce thermal shielding burden, and (2) maintain collected volatiles near cryogenic temperatures during post-extraction handling. HERMES therefore adopts a "rapid acquisition + immediate cryogenic capture" philosophy, centered on a triple-tube coring drill architecture and a simplified sample handoff path into a cryocooled rack.

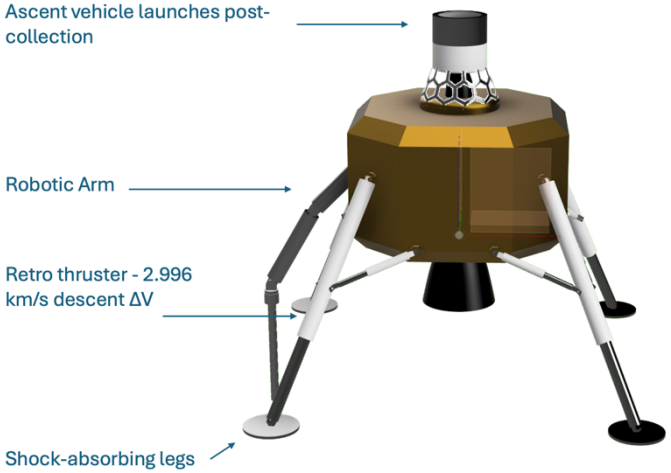

Figure 5: HERMES lander with deployed landing legs

The surface sampling and containment workflow proceeds as follows. A heritage-based robotic arm architecture (derived from Perseverance-class systems) is modified for HERMES to include 6 degrees of freedom (DOF) and a simplified end effector optimized for drilling and tube transfer. A rotary-percussive coring drill extracts sequential cores at target depths of 10 cm, 50 cm, and 100 cm. Following sample extraction, the arm routes the tube assembly to a fixed tube-catcher mechanism mounted on the lander deck. The catcher guides tubes into a 3-slot cryocooled rack, where each slot is thermally anchored to the cryocooler to suppress warming during storage and pre-launch operations.

The lander structure is also constrained by ascent vehicle integration. The Mercury Ascent Vehicle (MAV) must deliver a 25 kg payload from Mercury's surface to a 480 km orbit. The baseline mission parameters are GLOM = 700 kg, ΔV_{total} = 4.72 km/s, and Isp = 262 s. That means the lander must provide the launch support interface for the ascent vehicle while remaining stable and aligned during ignition and departure.

A first-order mass closure is taken from the Tsiolkovsky rocket equation:

$$\Delta V = I_{sp} g_0 \ln\left(\frac{m_o}{m_f}\right) \quad (1)$$

Using $\Delta V = 4.72 \times 10^3$m/s, $I_{sp} = 262$s, and $g_0 = 9.80665$m/s^2, the required mass ratio is:

$$\frac{m_0}{m_f} = \exp\left(\frac{\Delta V}{I_{sp} g_0}\right) = 6.28 \quad (2)$$

With $m_0 = 700$ kg, the implied final mass is mf = 111.5 kg, so the propellant mass is m_p = 588.5 kg. This ratio drives the lander layout. It sets the deck packaging, the launch restraint loads, and the load path through the lander structure during MAV support.

B. Structures and Mechanisms

1. Robotic arm architecture and loading environment

HERMES uses a compact robotic arm with a nominal reach of 1.2 to 1.5 m, sized to operate from a limited lander deck while supporting a rotary-percussive coring drill and tube-handling interface. The total end-effector mass is approximately 10 kg. Unlike the Mars 2020 Perseverance arm, which uses a 5-DOF configuration, the HERMES arm includes a sixth DOF at the wrist. This added roll axis allows precise drill alignment on uneven terrain within permanently shadowed polar regions. It reduces off-axis loading during core initiation and limits lateral force transfer into the arm structure.

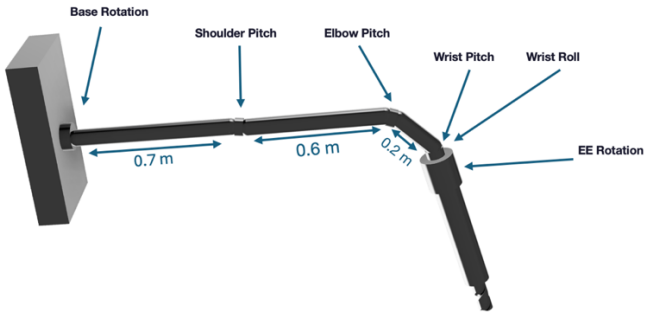

Figure 6: Robotic arm architecture.

Manipulator sizing is driven mainly by drilling loads. That includes the contact force during drilling, insertion and extraction forces, and the dynamic excitation from percussive operation. Early in the design, joint torques are estimated conservatively by modeling the arm as a serial cantilever with loads applied at the end effector.
For a given joint *j*, the minimum required actuator torque is written as:

$$T_j \geq \| r_j \times (F_{ext} + F_{drill}) \| + I_j \alpha_j + T_{friction} \quad (3)$$

Here, r_j is the vector from joint jto the drill contact point. F_{ext} represents the external loads at the end effector, including gravity, axial drilling force, and the drill assembly mass. F_{drill} accounts for reaction forces generated during drilling. I_j is the joint rotational inertia, α_j is the maximum joint angular acceleration, and $T_{friction}$ captures mechanical losses in the joint. The drilling reaction term is dominated by axial thrust and spindle torque and can be approximated as:

$$T_{drill,reaction} = F_{thrust} \cdot e_{offset} + T_{rotary} \quad (4)$$

where F_{thrust} is the design axial drilling force, taken as 800 N for ice-cemented regolith. The offset e_{offset} represents small misalignments between the drill axis and the surface normal, typically 0.01–0.02 m. T_{rotary} is the peak rotational torque transmitted through the spindle, set to 40 Nm. Under worst-case conditions, this produces a drilling-induced reaction torque of roughly 48–56 Nm at the wrist.

The arm uses a simple three-link serial layout. The link lengths are 0.7 m from shoulder to elbow, 0.6 m from elbow to wrist, and 0.2 m from the wrist to the drill tip, giving a total reach of about 1.5 m. Joint torques were estimated using worst-case static conditions with the arm fully extended horizontally under Mercury's gravity (3.7 m/s²). Each link was assumed to have a mass of 2.5 kg, with a 10 kg drill at the end. The resulting joint torque requirements are listed in Table 1.

Table 1: HERMES Robotic Arm Joint Torque Requirements

Joint	Function	Static Torque	Design Torque	Actuator Configuration
1	Base Rotation	55–70 Nm	120–150 Nm	BLDC + 160:1 Harmonic Drive
2	Shoulder Pitch	55–70 Nm	100–130 Nm	BLDC + 160:1 Harmonic Drive
3	Elbow Pitch	30–45 Nm	50–70 Nm	BLDC + 100:1 Harmonic Drive
4	Wrist Pitch	15–20 Nm	25–35 Nm	BLDC + 80:1 Harmonic Drive
5	Wrist Roll	8–12 Nm	15–20 Nm	BLDC + 50:1 Harmonic Drive
6	End-Effector Rotation	5–10 Nm	10–15 Nm	BLDC + 50:1 Harmonic Drive

Design torque values include a safety factor of 1.5 to 2.0 over static loading. This accounts for dynamic effects during drilling, joint acceleration while repositioning, and uncertainty in surface material properties. All joints use brushless DC motors paired with harmonic drive reducers for high torque density and zero backlash. Gear ratios range from 160:1 at the shoulder and elbow, where loads are highest, down to 50:1 at the wrist.

The arm links are baselined as either titanium alloy (Ti-6Al-4V) or carbon fiber composite to minimize mass while maintaining structural stability over the expected temperature range of −100°C to +50°C. Individual link masses are limited to 2 to 3 kg, resulting in a total arm mass of roughly 15–20 kg excluding the drill. This fits within the lander mass budget and provides adequate margin under combined gravitational, drilling, and inertial loads. A force-torque sensor at the wrist provides feedback during drilling, allowing real-time adjustment of feed rate and axial load to prevent bit stall or excessive wear.

Thermal control of the arm is handled passively through radiation and conductive coupling to the lander deck. Motors and electronics are rated for continuous operation at −100°C using space-qualified lubricants. Joint heaters are avoided to reduce power demand. Instead, thermal limits are managed by controlling duty cycles and allowing soak periods between drilling operations.

2. Triple-tube coring drill and breakoff retention

HERMES uses a triple-tube coring drill made up of an outer tube, a cutting tube, and a removable sample tube. This layout is chosen to preserve volatiles by limiting heat input during drilling and allowing fast transfer of the core into a thermally controlled storage path. The design is heritage-driven. The overall architecture follows RANCOR-style systems [13], while the core breakoff and retention approach is inspired by JPL's Praying-Mantis concept. The HERMES triple-tube coring drill assembly is shown in Figure 7.

The drill is a rotary-percussive system, similar to those flown on Curiosity and Perseverance. Rotary-percussive drilling has proven effective for penetrating consolidated regolith and rock on Mars while maintaining manageable power requirements. It is driven by a DC motor with an impact driver that delivers short bursts of high torque when resistance increases. This helps the drill handle ice-cemented regolith and local strength variations without excessive power draw. Before drilling begins, a self-tapping screw anchors the drill to the surface to limit lateral motion and reduce vibration caused by the eccentric cutting geometry.

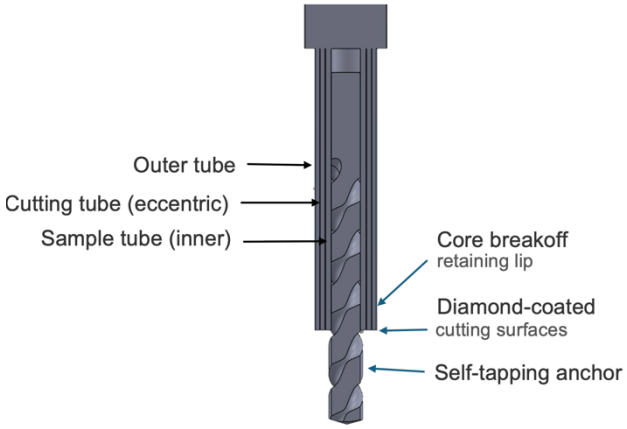

Figure 7: HERMES triple-tube coring drill assembly showing outer tube, eccentric cutting tube, and inner sample tube.

Cutting surfaces are specified as either diamond-coated tooling or tungsten carbide. Diamond tooling is preferred due to higher thermal conductivity, which helps move heat away from the cutting interface and reduce the risk of ice sublimation or melting. Diamond-coated drilling surfaces have also been widely used in planetary coring applications due to their durability and ability to maintain cutting performance in abrasive regolith environments. To further support volatile preservation, the core diameter is reduced compared to Mars heritage systems, with a target diameter of 10 to 15 mm. Smaller cores reduce conductive heat leak and cool faster once placed in cryogenic storage.

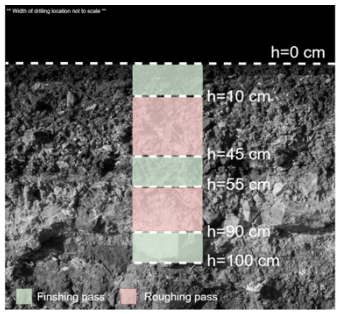

Figure 8: Stratified sampling strategy used for subsurface core collection [1]

The inner sample tube has a maximum volume of about 253 cm³. Assuming a bulk density of 4 g/cm³, a fully filled tube would collect roughly 1.0 kg of material over a continuous 35.8 cm cut. Rather than maximizing mass, HERMES focuses on stratified sampling. Cores are collected at depths of 10, 50, and 100 cm to capture volatile variation with depth. Within ±10 cm of each target depth, the drill switches to peck drilling with 2 cm increments to preserve layering. Outside these regions, higher-rate roughing passes are used to minimize total drilling time.

Drilling time is estimated using a simple feed-rate model based on depth removed per revolution. The total drilling time is written as:

$$\sum t = \Sigma \frac{\Delta h}{f_{rpl}} \tag{5}$$

where Δh is the incremental depth removed and f_{rpl} is the feed rate per revolution length. Rough drilling and sample collection are treated separately, giving:

$$\sum t = \Sigma \frac{\Delta h_{rough}}{f_{rpl,\,rough}} + \Sigma \frac{\Delta h_{finish}}{f_{rpl,\,finish}} \tag{6}$$

Using nominal feed rates of $f_{rpl,\,rough} = 2$ in/min for bulk material removal and $f_{rpl,\,finish} = 1$ in/min for sample collection, the total time required to reach and sample all three target depths is estimated at 66.93 minutes. This estimate excludes sample transfer and storage operations and fits within the mission's rapid surface operations timeline.

During drilling, the inner and outer tubes rotate about the same axis, but the cutting edge of the outer tube is intentionally eccentric. After sample collection, the outer tube is rotated in reverse by 180 degrees while a mechanical lock pin prevents the inner sample tube from rotating. This motion shears the base of the core and positions a retaining lip beneath it, mechanically securing the sample. The result is a clean breakoff and reliable retention during transfer into the lander's cryogenic storage system.

3. Sample unloading and Cryocooler

After a core is extracted, the robotic arm moves the loaded sample tube to a fixed tube-catcher mounted on the lander deck. The catcher is designed around three main goals: keep the mechanism simple, reliably capture and hold the tube in Mercury's low gravity (3.7 m/s²), and maintain a continuous thermal path into the cryocooled storage rack to limit sample warming during handoff.

The catcher itself is fully passive. The arm guides the tube into a funnel-shaped entry that centers the tube and constrains its motion as it is inserted. A tapered cone with a 15 to 20 degree half-angle transitions into a cylindrical guide sleeve sized to the tube's outer diameter. This geometry allows for small positioning errors while slowly increasing contact forces during insertion. A spring-loaded detent at the base of the sleeve locks the tube in place and prevents rebound or ejection once seated.

The force needed to insert a sample tube into the catcher is estimated using a basic friction model. That force has to overcome three things: the spring that locks the tube in place, friction between the tube and the guide sleeve, and any extra resistance if the tube is slightly misaligned. This relationship is written as:

$$F_{insert} \geq F_{preload} + \mu N + F_{misalign} \tag{7}$$

where $F_{preload}$ is the force from the detent spring that holds the tube once it is seated. It is kept low, around 10 to 20 N, so the tube is secure but still easy to insert. μ represents friction between the tube and the guide sleeve at cold operating temperatures and typically ranges from 0.1 to 0.3. N is the normal force caused by small alignment errors,

and $F_{misalign}$ accounts for added resistance if the tube enters at a slight angle. A force-torque sensor at the wrist of the robotic arm is used during insertion to monitor contact forces. If forces rise above about 50 to 80 N, the arm can stop or adjust the motion to avoid jamming or damaging the tube.

Once the tube is captured, the arm places it into one of three slots in a fixed cryogenic storage rack. This rack is directly connected to a pulse-tube cryocooler and held at about 123 K so the samples stay cold and do not sublimate during surface operations and ascent prep. Each slot is a machined aluminum sleeve which the tube enters. The rack is made from high-conductivity aluminum so heat can move out of the sample quickly and into the cryocooler. The tube makes direct contact with the rack, either through a tight fit or with thermal grease, to keep thermal resistance low and pull heat away as fast as possible.

The cryocooler is sized to keep the storage rack at 123 K, with a tolerance of ±5 K, even under worst-case thermal conditions. The main heat inputs come from three sources: heat conducted through structural supports and wiring, radiation from the surrounding lander and surface, and short-term heat added when a newly drilled core is inserted while still warm, on the order of 200 to 250 K.

To estimate the required cooling power, both steady-state and transient heat loads are considered. With three sample tubes and multi-layer insulation providing an effective emissivity of about 0.03, the steady-state radiative heat load can be estimated using:

$$Q_{rad} = \varepsilon_{eff}\sigma A\left(T_{surroundings}^4 - T_{rack}^4\right) \tag{8}$$

where, σ is the Stefan–Boltzmann constant, A is the effective radiating area of the rack, roughly 0.05 to 0.1 m², and $T_{surroundings}$ is taken conservatively as 300 K for worst-case analysis, even though permanently shadowed regions are much colder. Using these values, the radiative heat load is about 1 to 2 W.

Additional heat comes from conduction through mounts and cabling, which adds roughly 2 to 3 W. The largest short-term load occurs when a fresh core is placed into the rack and cooled from about 250 down to 123 K. During this period, the transient cooling load is estimated at 5 to 8 W. Adding these together gives a peak cooling requirement of roughly 10 to 15 W. This is well within the capability of available space-qualified pulse-tube cryocoolers in the 15 to 25 W range.

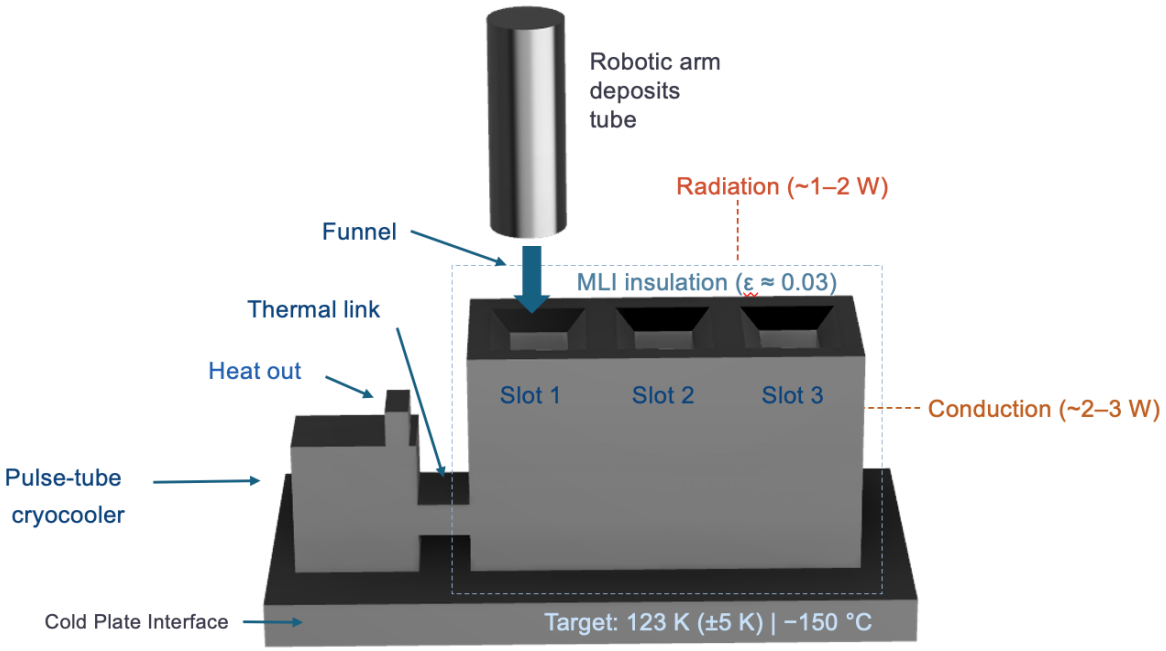

Figure 9: HERMES cryogenic storage rack with three-slot aluminum assembly, pulse-tube cryocooler, and MLI insulation.

The storage rack is fixed and does not rotate. This keeps the system simple, reduces mass, and avoids the added complexity of carousel-style sample handling. This approach works because surface operations are short, limited to a

single 2.3-hour orbit, and only three cores are collected. The robotic arm handles all tube placement, so there is no need for motors or active indexing inside the rack. Each slot includes a one-way retention feature, such as a spring-loaded pawl or ball detent, that allows the tube to be inserted but not removed. This keeps the samples secure during ascent and orbital rendezvous.

After all three samples are collected, the rack stays thermally connected to the lander cryocooler through final surface operations and ascent vehicle checks. Just before MAV ignition, the rack is mechanically separated from the lander cold plate and moved into the ascent vehicle payload bay. Once inside the MAV, it interfaces with a separate cryocooler that maintains temperature control through ascent, rendezvous, and return to Earth. This transfer causes a short thermal interruption, on the order of 2 to 5 minutes, but the thermal mass of the aluminum rack and residual cooling limit the temperature rise to less than 10 K, preserving sample integrity.

VI. Ascent Vehicle Design Details

A. System Architecture

After surface operations at Mercury's polar site, the collected ice samples are transferred into a cryogenic containment system and housed within the MAV. The primary objective of the MAV is to transport the sealed payload from the Mercury surface and rendezvous with the science orbiter operating in a circular 480 km altitude orbit. Due to Mercury's deep gravity well and lack of atmosphere, a two-stage solid rocket motor (SRM) architecture was selected to provide the required ascent performance with minimal system complexity and high reliability.

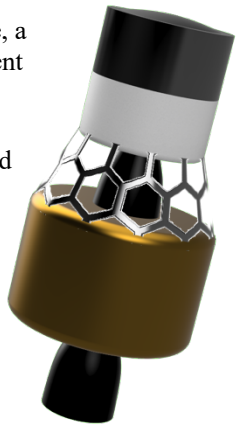

Figure 10: Mercury Ascent Vehicle (MAV)

Mission-level ascent requirements and baseline parameters used in the MAV design are summarized in Table 2 below:

Table 2: Ascent ΔV Requirement and Stage Allocation

Parameter	Symbol	Value	Units
Total Ascent ΔV	ΔV_{total}	4.72	km/s
Specific Impulse	I_{sp}	262	s
Payload Mass	$m_{payload}$	25	kg
Orbiter Altitude	h_{alt}	480	km

The total ascent ΔV required to transport the MAV from the Mercury surface to a 480 km circular orbit is estimated as:

$$\Delta V_{total} = 4.72 \text{ km/s}$$

This value includes orbital velocity insertion alone, with no gravity or steering losses being accounted for in the calculation. Atmospheric drag losses are also neglected due to Mercury's negligible atmosphere.

To minimize structural mass penalties while maintaining acceptable mass ratios for solid propulsion, the total ΔV was approximately evenly distributed across two stages:

$$\Delta V_{total} = \Delta V_1 + \Delta V_2 \quad (9)$$

$\Delta V_1 = 2.39$ km/s, $\Delta V_2 = 2.42$ km/s

The propulsion system employs SRMs with a specific impulse, based on the choice of propellant: Isp=262s.

Using the classical Tsiolkovsky rocket equation,

$$\Delta V = g_0 I_{sp} ln(f_0) \left(\frac{m_0}{m_f}\right) \quad (10)$$

where m_0, m_f are the initial and final masses of each stage, respectively, the corresponding mass ratios were obtained: $(m_0/m_f)_1 = 2.53$, $(m_0/m_f)_2 = 2.6$.

The resulting mass allocation for both of these stages is given below:

Table 3: Propellant Mass Estimation and Mass Budget

Metric	Stage 1	Stage 2

Initial Mass	695.24 kg	279.52 kg
Dry Mass	274.76 kg	106.86 kg

Using the computed mass ratios and payload constraints, propellant mass estimates were derived iteratively for both stages. The total Gross Lift-Off Mass (GLOM) of the MAV was constrained to 700 kg to remain compatible with the lander structural and deployment limits.
The propellant mass for each stage is given by:

$$m_{prop} = m_0 - m_{dry} \tag{11}$$

The total propellant mass required for ascent is:

$$m_{prop,total} = 588.38 \text{ kg}$$

Resulting propellant allocations are summarized below:

Table 4: Propellant mass

Stage	Propellant Mass
Stage 1	420.48 kg
Stage 2	167.90 kg
Total	588.38 kg

Leaving sufficient margin for structural dry mass, avionics, thrust structure, and payload accommodation. The final delivered payload mass to orbit, including the cryogenically preserved ice samples, is 25 kg.

VII. Earth Return Vehicle

The Earth Return Vehicle must complete the final leg of the mission. By this point, much of the mission hardware will have been left behind after it has served its purpose in order to save mass. The return vehicle must ensure that the ice samples are protected from harmful solar radiation in Mercury orbit to the intense heating of reentry into Earth's atmosphere. To achieve this, a multi-layered approach will be taken to ensure the integrity of the samples. The samples themselves will be stored in a cryocooler located within the reentry capsule, which must be sufficiently insulated so that the cryocooler does not overheat and the samples remain cold until they can be transferred to a more permanent storage location on Earth. The return vehicle will make use of a multi-layer kapton sun shield similar to the one deployed on the James Webb space telescope in order to prevent excessive solar heating.

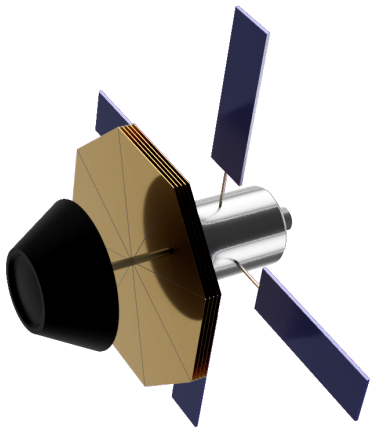

Figure 11: Earth Return Vehicle with sun shield

Additionally, the return vehicle will include a propulsion module, which will be tasked with generating the necessary power for the cryocooler and other subsystems using solar panels, as well as performing the capture and deorbit burns once the craft reaches Earth. The capsule will make use of a standard phenolic impregnated carbon ablative heat shield for reentry, and the final descent will be controlled using parachutes.

VIII. Conclusion

The HERMES platform promises to be a very versatile and highly capable system. Using this mission architecture, a Mercury surface landing, sample collection, and sample could all be completed within just a single mission, eliminating the need for a separate costly sample return mission. In addition to the samples, the mission would also pose an opportunity to gather close-up data on what is now a relatively understudied world. This would be of great utility not only to studying Mercury but could also be adapted to many other celestial bodies within the solar system, allowing for an unprecedented look into material which could hold information about the solar system's distant past.

Acknowledgments

The authors would like to greatly acknowledge the work of the past HERMES team members led by Hadley Douglas, and the outstanding mentorship they have received from Dr. Steve Matousek from NASA-Jet Propulsion Laboratory. Special thanks to the CRASH Lab graduate students who provided support to the team, Samyak Mehta and Guru Teja.

References

[1] Douglas, H., Leader, E., Fish, L., Govoni, M., Mehta, S., and Bayandor, Dr. J., "Exploration of hermean polar ice," *2025 Regional Student Conferences*, Aug. 2025.
[2] Kosambe, Santosh. "Chandrayaan-2: India's Second Lunar Exploration Mission." Science Publications, thescipub.com/pdf/jastsp.2019.221.236.pdf. Accessed 26 Feb. 2026.
[3] "Cassini-Huygens Operations." ESA, 4 Dec. 2006, www.esa.int/Enabling_Support/Operations/Cassini-Huygens_operations#:~:text=to%20the%20surface.-,The%20descent%20phase%20lasted%20around%202%20hours%2C%2027%20minutes%2C%20with,least%203%20minutes%20on%20ground).
[4]"Huygens Probe Separation and Coast Phase - Cassini-Huygens - Science Portal." Cassini-Huygens, 1 Sept. 2019, sci.esa.int/web/cassini-huygens/-/34956-huygens-probe-separation#:~:text=Following%20the%20turn%20to%20the,per%20second%20on%20all%20axes.&text=Once%20the%20separation%20command%20is,telemetry%20recorded%20for%20later%20playback.
[5] Hoffpauir, Daniel. "Space Rendezvous." NASA, NASA, 23 May 2016, www.nasa.gov/centers-and-facilities/nesc/space-rendezvous/#:~:text=There%20is%20also%20the%20possibility,Mr.
[6] Ajluni, Thomas, et al. NASA, ntrs.nasa.gov/api/citations/20150000809/downloads/20150000809.pdf?attachment=true. Accessed 28 Feb. 2026.
[7] "Huygens Landing Spin Mystery Solved." ESA, 14 Jan. 2020, www.esa.int/Science_Exploration/Space_Science/Cassini-Huygens/Huygens_landing_spin_mystery_solved#:~:text=However%2C%20one%20thing%20remained%20a,eventually%20entered%20the%20moon's%20atmosphere.
[8] Christian, John A., and Scott Cryan. "A Survey of LIDAR Technology and Its Use in Spacecraft Relative Navigation." NASA, ntrs.nasa.gov/api/citations/20140000616/downloads/20140000616.pdf. Accessed 27 Feb. 2026.
[9] Landis, Geoffrey A. "Solar Power for Near-Sun, High-Temperature Missions." NASA, 2008, ntrs.nasa.gov/api/citations/20090004578/downloads/20090004578.pdf.
[10] Ercol, C. Jack. "MESSENGER Heritage: High-Temperature Technologies for Inner Solar System Spacecraft." JHUAPL, 2007, messenger.jhuapl.edu/Resources/Publications/Ercol.2007.pdf.
[11] Home, William D., et al. ."., Telecommunications for Mars Rovers and Robotic Missions William D. Home." Oup, global.oup.com/us/companion.websites/fdscontent/uscompanion/us/pdf/houp/rover.pdf. Accessed 28 Feb. 2026.
[12] "Mercury Planetary Orbiter - Spacecraft - Bepicolombo - Science Portal." BepiColombo, 30 Mar. 2020, sci.esa.int/web/bepicolombo/-/48872-spacecraft#:~:text=Communications,for%20use%20during%20special%20campaigns.
[13] Paulsen, G., Indyk, S., and Zacny, K., "Development of the RANCOR Rotary-Percussive Coring System for Mars Sample Return" *NASA Technical Reports Server,* May. 2014
[14] Jehn, R., and Schoenmaekers, J., "BepiColombo Trajectory Options to Mercury in 2016 and 2017" *ISSFD, https://www.issfd.org/ISSFD_2014/ISSFD24_Paper_S6-5_jehn.pdf*
[15] Design of Rockets and Space Launch Vehicles - Don Edberg, Willie Costa